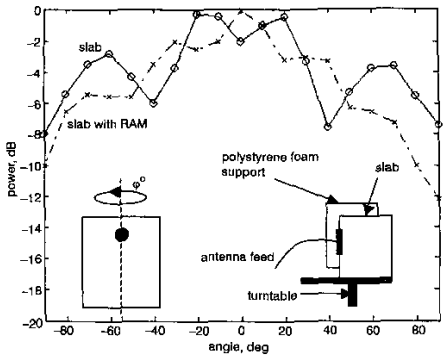

a

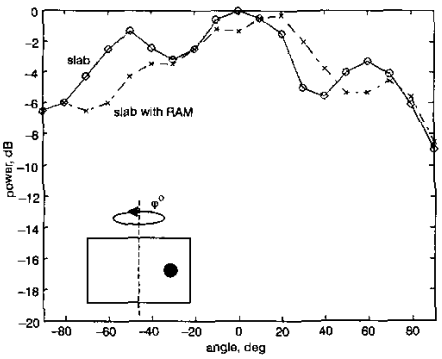

b

Fig. 2 *Radiation patterns of flush mounted patch antenna on thermalite slab ($2t = 100$ mm) at $f_0 = 2.03$ GHz*
a H-plane; *b* E-plane

In a second experiment, a microstrip patch antenna was attached directly to a thermalite block (440 × 215 × 100 mm) and the dipole-like radiation patterns measured in an anechoic chamber. The results given in Figs. 2*a* and *b* show the effect of placing radar absorbent material (RAM) on the block ends to absorb the surface wave contribution. With no absorbent material the surface waves result in some secondary radiation at the block ends thus creating a ripple interference pattern. The surface wave excitation is clearly a polarisation-dependent propagation mechanism.

Discussion and conclusions: Surface wave propagation on walls has been theoretically and experimentally demonstrated for some typical building materials. The water content of the material has pronounced effect on the parameters. Field reinforcement near dry wall surfaces is likely to occur in practical WLAN scenarios, both around and within buildings. Ray-tracing and other field prediction techniques may require modification to account for the surface wave fields and the complex interactions taking place.

Acknowledgments: Helpful discussions with R. Craven (DSTL) and P. Nobles (RMCS) are gratefully acknowledged.

28 November 2002
Electronics Letters Online No: 20030122
DOI: 10.1049/el:20030122

J.R. James and I.L. Morrow (*Laboratory of Electromagnetic Research, Department of Aerospace, Power and Sensors, Cranfield University, RMCS, Shrivenham, Swindon, Wilts., SN6 8LA, United Kingdom*)

P. Cushnaghan and A.S. Fairweather (*Defence Science Technology Laboratory (DSTL), Malvern, Worcs., WR14 3PS, United Kingdom*)

References

1 ZHANG, Z., SORENSEN, R., YUN, Z., ISLANDER, M., and HARVEY, J.F.: 'Ray tracing approach for indoor/outdoor propagation through window structures', *IEEE Trans. Antennas Propag.*, 2002, **50**, (3), pp. 742–749
2 European Committee COST-231: 'Digital mobile radio: COST-231 view on the evolution towards 3rd generation systems', Final report, European Commission, Brussels, Belgium, 1998
3 SANTAMARIA, A., and LOPEZ-HERNADEZ, F.J.: 'Wireless LAN systems' (Artech House, London, 1993), Chap. 6
4 BARLOW, H.M., and BROWN, J.: 'Radio surface waves' (Oxford University Press, London, 1962)
5 COLLINS, R.E.: 'Field theory of guided waves' (IEEE Press, 1991, 2nd edn.), Chap. 11
6 CLEMMOW, P.C.: 'Plane wave spectrum presentation of electromagnetic fields' (Pergamon Press, New York, 1966)
7 BRAMANTI, M., and SALERNO, E.: 'Experiments on some particular permittivity sensors in non-destructive testing of dielectric materials', *J. Electromagn. Power Microw. Energy*, 1992, **12**, (4), p. 209

Modelling noise and delay in VLSI circuits

D. Pamunuwa, S. Elassaad and H. Tenhunen

New models for estimating delay and noise in VLSI circuits, based on closed form expressions for the first and second moment of the impulse response in coupled *RC* trees are reported. The effect of crosstalk on delay and noise can be accurately estimated with a complexity only marginally higher than the Elmore delay.

Timing analysis in VLSI circuits has long used the simple model of an *RC* tree where all capacitors are connected to ground, which we shall call a *simple* tree. Signal delay through the tree is usually estimated by approximating the dominant time constant with the Elmore delay [1], the first moment of the impulse response. For waveforms which are poorly represented by a single exponential, a two pole, single zero model based on the first two moments and the sum of the open circuit time constants was proposed in [2]. Generic moment matching techniques were later derived in [3], which could be applied for any type of circuit with linear elements. Recently [4] and [5] have presented alternate second-order models for the transfer function, using the first three moments, and the first two moments with heuristics, respectively. With the increased integration allowed by nanometre processes, noise coupling has become very important, and the circuit model has to include coupling capacitors. In estimating the delay in such *coupled* trees, the usual practice is to modify the Elmore delay by an empirical coefficient [6] which however results in poor accuracy. General moment matching can be applied, but for initial analysis that requires many iterations, the formulation of the nodal matrices and subsequent costly matrix manipulations are best avoided, even for models which depend on only the first three or four moments [7].

In this Letter, we report second-order models for general arbitrarily-coupled trees with multiple drivers that depend only on the first two moments of the circuit, which moreover are explicitly matched to the circuit elements by means of closed form equations. Our models can be thought of as an extension of the methodology presented in [2], to coupled trees, and represent the minimum complexity with which second-order approximations can be obtained without compromising generality. The response for each driver switching is obtained by grounding all other inputs. The superposition of all waveforms allows accurate delay and noise estimations.

The circuit topology consists of simple trees coupled to each other through series capacitors, and an example is shown in Fig. 1. The notation we employ is that CS_k^p is the capacitance to ground at node k in the pth tree, CC_{kj}^{pq} is the capacitance between node k on the pth tree and node j on the qth tree where the first sub(super)script refers to the reference tree, R_{ke}^p is the resistance shared on the paths between the source and nodes e and k, respectively, on tree p, and Υ_k^n is the nth moment of the impulse response at the kth node. Superscripts always refer to simple trees while subscripts always refer to nodes, except in the definition for moments, where the superscript refers to the order of the moment. Additionally, rail voltages are normalised to 0 and 1, and the expressions derived for a positive step without loss of generality.

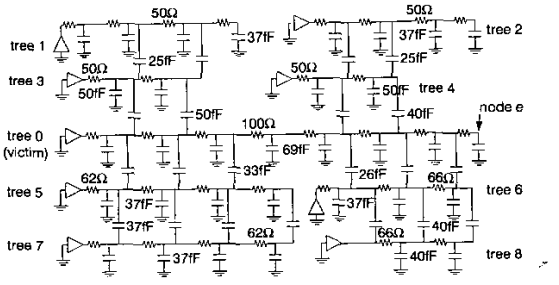

Fig. 1 *Coupled RC tree (values repeated within simple trees)*

A coupled *RC* tree is characterised by a resistive path from the receiver node e to the forcing (victim) driver, and series capacitive elements to other (aggressor) drivers. Hence when the victim driver switches the output will always change rails, whereas it will start and end at the same rail for an aggressor switching. Therefore the second-order transfer function for the former case will have a zero on the negative part of the real axis:

$$H_v(s) = \frac{1 + s\tau_{z,v}}{(1 + s\tau_1)(1 + s\tau_2)} \tag{1}$$

and at the origin for the latter:

$$H_{a_i}(s) = \frac{s\tau_{z,a_i}}{(1 + s\tau_1)(1 + s\tau_2)} \tag{2}$$

Using Kirchoff's laws and integration by parts, the first moment of the impulse response at e for the victim driver switching is seen to be:

$$\Upsilon_e^1 = \sum_{k \in victim} R_{ke}^v [CS_k^v + CC_k^{va_1} + CC_k^{va_2} + \cdots] = \tau_{D_e}^v \text{ say} \tag{3}$$

Similarly, the second moment is:

$$\Upsilon_e^2 = 2 \sum_{k \in victim} R_{ke}^v \left\{ CS_k^v \tau_{D_k}^v + CC_k^{va_1} \left[\tau_{D_k}^v + \sum_{K \in a_1} R_{Kj}^{a_1} CC_K^{a_1 v} \right] + CC_k^{va_2} \left[\tau_{D_k}^v + \sum_{K \in a_2} R_{Kj}^{a_2} CC_K^{a_2 v} \right] + \cdots \right\} = 2(\tau_{G_e}^v)^2 \text{say} \tag{4}$$

The first moment at node e for aggressor a_i switching is:

$$\Upsilon_e^1 = -\sum_{k \in victim} R_{ke}^v CC_k^{va_i} = -\tau_{D_e}^{a_i} \text{ say} \tag{5}$$

The second moment is:

$$\Upsilon_e^2 = -2 \sum_{k \in victim} R_{ke}^v \left\{ (CS_k^v + CC_k^{va_1} + CC_k^{va_2} + \cdots)\tau_{D_k}^{a_i} + CC_k^{va_i} \left[\sum_{K \in a_i} R_{Kj}^{a_i} (CS_K^{a_i} + CC_K^{a_i v} + CC_K^{a_i b_1} + \cdots) \right] \right\} = -2(\tau_{G_e}^{a_i})^2 \text{ say} \tag{6}$$

The moments are matched to the characteristic time constants in the circuit by using the identity that the nth moment of the impulse response is $(-1)^n$ times the nth derivative of the transfer function evaluated at $s = 0$. When applied to (1), (3) and (4), this results in (7) and (8):

$$\tau_{D_e}^v = \tau_1 + \tau_2 - \tau_{z,v} \tag{7}$$

$$(\tau_{G_e}^v)^2 = (\tau_1 + \tau_2 - \tau_{z,v})(\tau_1 + \tau_2) - \tau_1\tau_2 \tag{8}$$

Now τ_1 and τ_2 in (7) and (8) refer to the dominant poles for the event of the victim driver switching. To solve this system of three unknowns, a third equation is required. Since all aggressors are grounded, the metric that gives the best solution is the sum of the open circuit time constants with reference to the victim driver, which we shall call τ_p^*. This is a good approximation for the sum of the pole time constants, giving:

$$\tau_p^* = \tau_1 + \tau_2 \tag{9}$$

Now (7), (8) and (9) can be solved for the zero and two poles associated with the victim switching.

To solve for the poles and zeros associated with an aggressor switching, the above identity is used on (2), (5) and (6) to give:

$$\tau_{D_e}^{a_i} = \tau_{z,a_i} \tag{10}$$

$$(\tau_{G_e}^{a_i})^2 = \tau_{z,a_i}(\tau_1 + \tau_2) \tag{11}$$

Now the zero is available immediately, and dividing (11) by (10) results in the pole sum:

$$\frac{(\tau_{G_e}^{a_i})^2}{\tau_{D_e}^{a_i}} = \tau_1 + \tau_2 \tag{12}$$

Again, the solution for the poles requires extra information, which can be obtained by using intuition gained from the physical interpretation of the moments. The first moment includes resistances of the switching line, and either all capacitances connected to it (when the victim switches) or capacitances connecting it to a particular line (when an aggressor switches). The second moment propagates outwards another level, and includes resistances and capacitances of immediately adjacent lines as well. Since the victim is the net of interest, combining the moments for the victim switching with those for a particular aggressor switching results in a solution which is biased towards the victim and that aggressor. Hence to obtain the solution to a switching aggressor, (7), (8) and (12) can be combined to generate the two poles of interest.

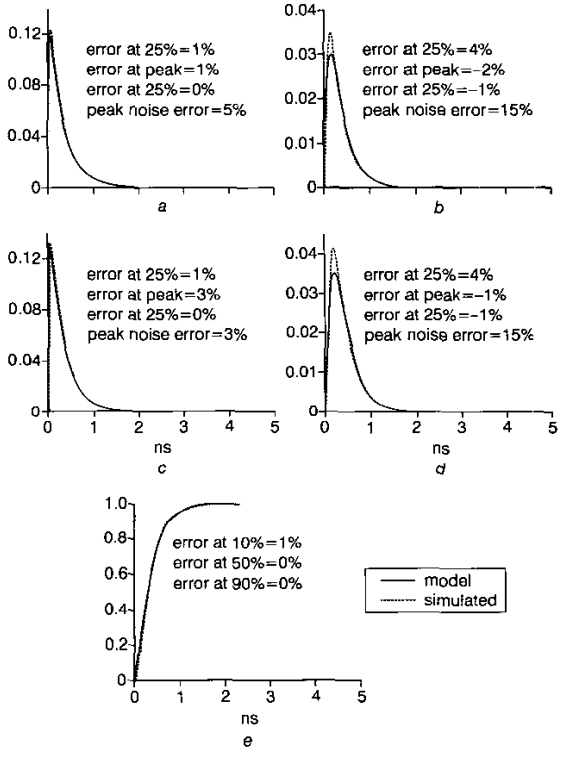

Fig. 2 *Response at output node e for switching of different drivers*

a Response of aggressor tree 4
b Response of aggressor tree 3
c Response of aggressor tree 6
d Response of aggressor tree 5
e Response of victim

The accuracy of the models for the transfer function were tested by comparing the step responses for a variety of circuits against a dynamic simulator Spectre, and found to be excellent for the vast majority. The waveforms shown in Fig. 2 correspond to the circuit of Fig. 1. For certain pathological cases where the significant poles for a switching aggressor are located very far away from those of the victim, this methodology can fail to generate real poles for the aggressor. Such an

occurrence is an indication that the receiver node is charged via a strong aggressor, i.e. through a relatively very small time constant, and decays with a very long tail, dictated by the much larger time constant of the victim. One remedy would be to use the third moment of the impulse response to gather extra information, and use a technique that guarantees stability, similar to that described in [4], just for those corner cases. Another would be to consider simple circuit transformations, as any instability is an indication that the response is dictated by a very limited section of the overall circuit for that particular case. However for almost all of the topologies tested by the authors, the methodology described gave stable and accurate results. The simplicity and accuracy of the models combined with their generality should make them useful in delay and noise estimations in complex systems, early in the design flow.

5 November 2002
Electronics Letters Online No: 20030208
DOI: 10.1049/el:20030208

D. Pamunuwa and H. Tenhunen (*Department of Microelectronics and Information Technology, Royal Institute of Technology (KTH), Electrum 229, SE-16440 Stockholm-Kista, Sweden*)

E-mail: dinesh@imit.kth.se

S. Elassaad (*Cadence Berkeley Laboratories, Cadence Design Systems, 2001 Addison St., Berkeley, CA 94704, USA*)

References

1 ELMORE, W.C.: 'The transient response of linear damped circuits', *J. Appl. Physics*, 1948, **19**, pp. 55–63
2 HOROWITZ, M.A.: 'Timing models for MOS circuits'. PhD Thesis, Stanford Electronics Laboratories, Stanford University, Stanford, CA, USA, January 1984
3 PILLAGE, L.T., and ROHRER, R.A.: 'Asymptotic waveform evaluation for timing analysis', *IEEE Trans. Comput.-Aided Des. Integr. Circuits Syst.*, 1990, **9**, pp. 352–366
4 TUTUIANU, B., DARTU, F., and PILLAGE, L.T.: 'An explicit RC-circuit delay approximation based on the first three moments of the impulse response'. Proc. ACM/SIGDA Design Automation Conf. (DAC), USA, 1996 pp. 611–616
5 ALPERT, C.J., DEVGAN, A., and KASHYAP, C.V.: 'RC delay metrics for performance optimization', *IEEE Trans. Comput.-Aided Des. Integr. Circuits Syst.*, 2001, **20**, (5), pp. 571–582
6 KAHNG, A.B., MUDDU, S., and SARTO, E.: 'On switch factor based analysis of coupled RC interconnects'. Proc. ACM/SIGDA Design Automation Conf. (DAC), USA, 2000, pp. 79–84
7 ACAR, E., ODABASIOGLU, A., CELIK, M., and PILLAGE, L.T: 'S2P: a stable 2-pole RC delay and coupling noise metric'. Proc. ACM/SIGDA Great Lakes Symp. on VLSI (GLSVLSI), USA, 1999, pp. 60–63

Watkins-Johnson converter completes tapped inductor converter matrix

D.A. Grant and Y. Darroman

The Watkins-Johnson converter has been identified as belonging to the tapped inductor converter families extending once more the matrix of DC-DC converter topologies. This converter is analysed in terms of the tap position and the switch duty cycle and its operation as a rail-to-tap buck converter is verified.

Introduction: Tapped inductor DC-DC converters are well-known [1, 2]. They are often used in industrial and domestic applications because they facilitate high or low output-to-input voltage ratios with good efficiency if there is no requirement for isolation. Moreover tapping the inductor has the benefits that the duty cycle of the converter at the operating point can be adjusted to a desirable value-typically a value at which device utilisation is improved. The tapping of the inductor also permits a different mix of voltage and current ratings for the various elements of the circuits.

Filling the void in tapped inductor matrix: Recent work on these converters has shown that tapped and untapped versions of the DC-DC converter formed a matrix of possibilities to which a new column was added with two new converter members [3, 4]. This categorisation left a void in the matrix at the position assigned to the buck converter of the rail-to-tap configuration. We now believe that the Watkins-Johnson converter [5–10] is the best candidate to fill this void. In [10] it is referred to as a buck converter with desirable properties – in particular, on switch-off, the isolation from the output of any energy stored in the inductor.

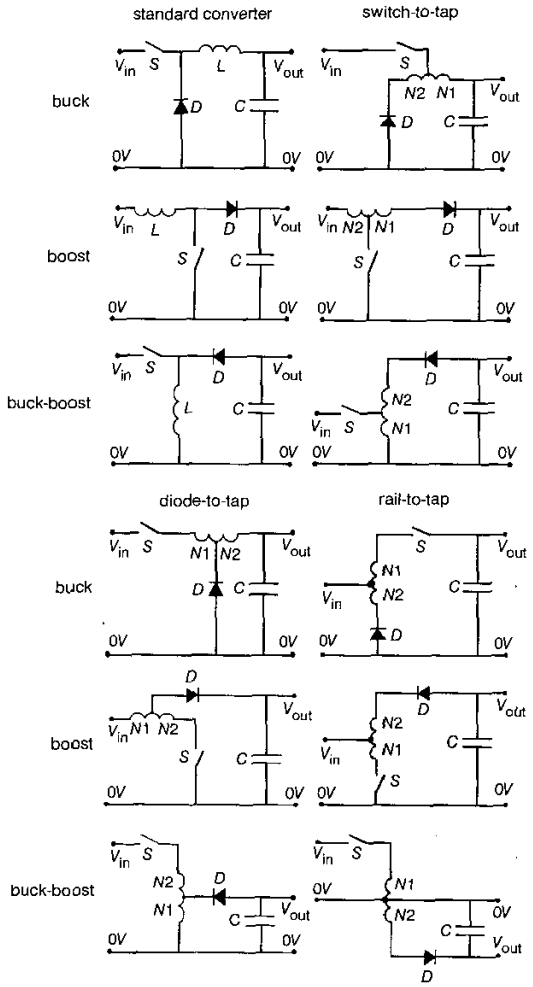

Fig. 1 *Tapped inductor family of converters; converter circuits*

Table 1: Tapped inductor family of converters; voltage transfer ratios

Converter type	No tap	Switch-to-tap	Diode-to-tap	Rail-to-tap
Buck	δ	$\delta/(K+\delta(1-K))$	$K\delta/(1+\delta(K-1))$	$(\delta-K)/\delta(1-K)$
Boost	$1/(1-\delta)$	$(K+\delta(1-K))/K(1-\delta)$	$(1+\delta(K-1))/(1-\delta)$	$(K-\delta)/K(1-\delta)$
Buck-boost	$-\delta/(1-\delta)$	$-\delta/K(1-\delta)$	$-K\delta/(1-\delta)$	$(1-K)\delta/K(1-\delta)$

The transfer ratios V_{out}/V_{in} (in continuous conduction mode) of the converters shown in Table 1 and the basic power circuits of each converter are shown in Fig. 1. The Watkins-Johnson converter (or rail-to-tap buck converter) is highlighted in these Tables. The transfer ratio for the Watkins-Johnson converter indicates that it can buck without inversion of polarity. In this mode it can supply a passive load (positive output voltage and positive output current). It can buck and boost with polarity inversion although in this regime an active load is required since the output current must remain positive even though the output voltage is negative. Hence, with the classification scheme employed